POLITECNICO
MILANO 1863

SCUOLA DI INGEGNERIA INDUSTRIALE
E DELL'INFORMAZIONE

Executive Summary of the Thesis

Design and optimization of a point focus Beam-Down system

Laurea Magistrale in Energy Engineering - Ingegneria Energetica

Author: Andrea Zanut

Advisor: Prof. Andrea Giostri

Co-advisor: Prof. Marco Binotti

Academic year: 2020-2021

1. Introduction

In CSP applications, Beam-Down optics (BD) can play a major role in the future decarbonized energy scenario. The presence of a ground-mounted receiver avoids moving the working fluid from the tower up to the power block and therefore decreases the thermal and pumping losses. The BD optic is composed mainly of the heliostat field, a Secondary Reflector (SR), a possible tertiary concentrator, and a receiver. Two different foci characterize the system optic, an upper one that coincides with the aim point of the heliostat field, and a lower one that corresponds to the entrance of the tertiary concentrator, generally a Compound Parabolic Concentrator (CPC), or if it's not the case, directly with the receiver aperture as shown in Figure 1.

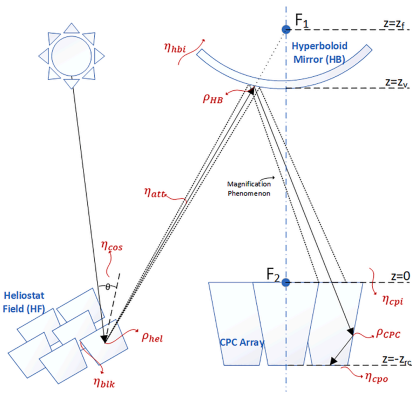

Figure 1: Beam down optic [39].

The secondary reflector considered in this work was of hyperbolic shape. As reported in the literature, it guarantees higher optical performances concerning the elliptical one [43].
A circular two-sheet hyperboloid is generally expressed by the simplified canonic form in Equation 1.

$$\frac{x^2}{a^2} + \frac{y^2}{a^2} - \frac{z^2}{b^2} = -1 \tag{1}$$

Considering a two-sheet hyperboloid, an important parameter utilized in a BD system to identify one specific surface among the infinite ones is the eccentricity, defined as Equation 2.

$$e = \frac{FocDist/2 + b}{FocDist} \tag{2}$$

Where $FocDist$, as shown in Figure 1, is the distance between the upper and the lower focus and b is the semi-minor axis.
The value of eccentricity for a two-sheet hyperboloid is always greater than one. As the eccentricity increase, as shown in Figure 2, the hyperboloid crushes to half of the focal distance, and its radius increase to catch the farthermost light point coming from the heliostat field.
Another important geometric parameter to consider in designing BD systems is the CPC entrance acceptance angle, measured from the CPC longitudinal axis. If the ray incidence angle θ_i is higher than the maximum one allowed by the CPC, θ_{max}, the ray will be rejected and so won't be collected by the receiver.

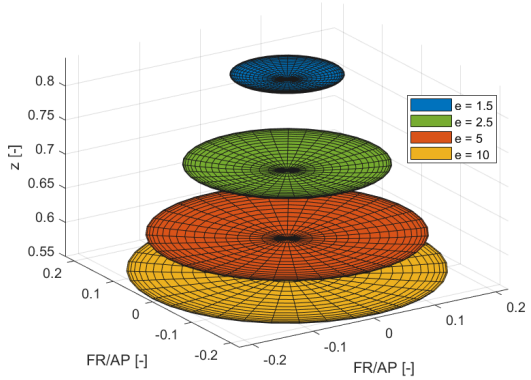

Figure 2: 3D representation of hyperboloid at different eccentricity values.

The theoretical 3D Concentration Ratio ($CR_{cpc,3D}$) of the CPC can be evaluated as Equation 3.

$$CR_{cpc,3D} = \frac{1}{(sin\ \theta_{max})^2} \tag{3}$$

Following geometrical consideration, the higher will be the secondary reflector eccentricity, the higher will be the maximum incidence angle into the CPC aperture, and so the lower the concentration ratio.

Current installed BD optic solar fields are made out of a circular surrounded pattern.
This work aims at investigating the possibility of generating an asymmetrical heliostats field, so to exploit the most performing area of the site, in terms of cosine, at latitudes far from the equator.
Furthermore, it was chosen to perform the analysis for a 50 MW_{th}, at receiver aperture, solar field at a latitude of 25° North. Nevertheless, the presented algorithm can be applied to any latitude and design power.
It was proven that the most optical performing area of the solar site in conventional solar tower systems, is strongly influenced by the shadow of the hyperboloid and that the replacement of mirrors in that part of the field, with farther ones less shaded, can increase the annual optical performance.
On the other hand, the farther heliostat selection is limited by the geometry of the CPC, and therefore an optimization methodology is presented, to maximize the annual optical-thermal performance of the system at different eccentricity values and aim point heights, in order to find the best solar field configuration.
Moreover, a 1D thermal model for the SR is lastly presented to roughly assess the temperature distribution at the secondary reflector surface and possible configurations to limit the silver reflective film temperature to its maximum operating value.

2. Methodology

2.1. Heliostat field creation

A possible heliostats field configuration can be the one of a radial staggered. Two main parameters identify the disposition of the mirrors, the azimuthal distance ΔAz and the radial displacement ΔR. The design considered has the main advantage of easy blocking heliostat individuation. In order to generate the heliostats field in Matlab, the *campo* code developed by Collado et al. [13], was utilized. Furthermore, the DELSOL3 correlation was considered for the radial spacing between rows [22]. The heliostats were assumed made out of one facet, rectangular, and with a dimension of 5x5 m.

2.1.1 Heliostat performance

Different types of losses take place in the ray path from the sun towards the receiver and so an optical efficiency can be defined for each i-mirror.
The latter, in the case of a BD system, is presented as Equation 4.

$$\eta_{opt,i} = \rho_{helio} \cdot \rho_{SR} \cdot \eta_{cos,i} \cdot \eta_{S\&B,i} \cdot \eta_{int,i} \cdot \eta_{s,SR,i} \tag{4}$$

New terms like ρ_{SR} (SR reflectivity) and $\eta_{s,SR}$ (SR shadow efficiency) appear in the BD applications, concerning solar towers, due to the presence of a secondary reflector.

Shadowing and Blocking (S&B) The S&B performance evaluation was implemented in Matlab utilizing the Sassi method [40], as shown in Figure 4. This type of loss, as the cosine one, is sun position-dependent and related to the reciprocal position of the i-mirror over the one of the K-neighbours.
For this reason, the S&B efficiency is the most energivourous in terms of computational time.

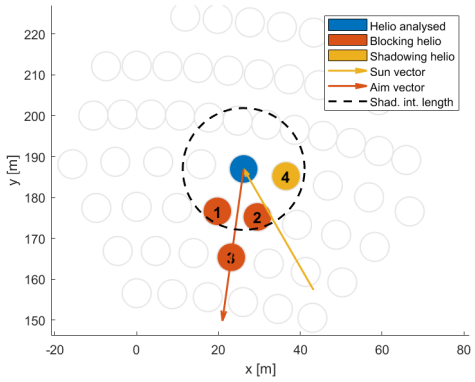

Figure 3: Shading and blocking heliostats selection.

Nevertheless, the radial staggered configuration guarantees easy blocking mirrors individuation. Taking into consideration a generic i-heliostat, three blocking k-heliostat can be easily found, two in front on

the first inner row, named shoulders, and one directly in front in the second inner row, named nose. This is not strictly true for heliostat living in the first row (missing direct nose and shoulder association) or the second row of a new compressed row (missing the nose). The arrangement of the mirrors is changed and the identification of the interfering heliostat has to be made by distances consideration. The same procedure was utilized for possible shadow candidates. The only difference is that blocking selection is based on the aiming vector of the i-heliostat $\vec{\mathbf{a_i}}$, while for shadowing the sun vector pointing at the i-heliostat at a given sun position, $\vec{\mathbf{s_i}}$, is considered.
Let's consider a vector $\vec{\mathbf{t_i}}$, that can be either $\vec{\mathbf{a_i}}$ for blocking performance or $\vec{\mathbf{s_i}}$ and a i-heliostat defined by its normal vector $\vec{\mathbf{n_i}}$ such that $\vec{\mathbf{s_i}} + \vec{\mathbf{a_i}} = \vec{\mathbf{n_i}}$.
It's possible to calculate a length of interaction for the i-heliostat, as shown in Figure 3, that represents the farthest mirror projection point onto the ground in a 2D plane by solving the system of a straight line passing from the highest point of the heliostat and a plane at $z = 0$, as presented in Equation 5.

$$L_{int} = \frac{\left(h_i + \frac{DM}{2}\sin\theta\right) \cdot \sqrt{t_x^2 + t_y^2}}{t_z} + DM\cos\theta_z \quad (5)$$

Where DM is the mirror diagonal, h_i the installation height and θ_z the zenit angle of $\vec{\mathbf{n_i}}$. If a heliostat lies at a distance smaller than the interaction one, it can possibly interfere with the i-mirror considered.

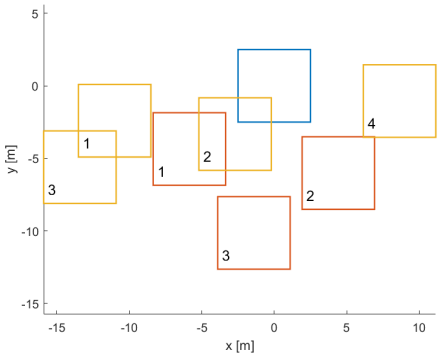

Figure 4: Shadowing and blocking performance evaluation. Interfering heliostats number as Figure 3.

Intercept factor The intercept efficiency was assessed by generating a random distributed number of rays on the mirror surface, intersecting them with the secondary reflector, and bouncing them on a selected CPC geometry. All the ray bounces consider optical error perturbation as Table 1.
Due to the presence of a CPC, the intercept efficiency was evaluated as the number of rays that fall inside a specific CPC inlet radius with an incidence angle lower than the maximum one, over the total number of generated rays.

Property	Value [mrad]	Description
σ_{sun}	4.1	Sun shape error
σ_{slope_f}	1.53	Heliostats field slope error
σ_{spec_f}	0.2	Heliostats field specularity error
σ_{slope_h}	1.53	Hyperboloid slope error
σ_{spec_h}	0.2	Hyperboloid specularity error

Table 1: Values of sun shape, slope and specularity errors considered. Values from default SolarPILOT configuration.

Hyperboloid shadow Another loss introduced by a BD system with respect to a conventional solar tower is the one relative to the shadow formed by the secondary reflector. This effect cannot be neglected, especially for a high value of eccentricity, so when the hyperboloid is bigger, squeezed at half of the focal distance.
Given a sun position and a i-mirror with normal $\hat{\mathbf{n}}_\mathbf{i}$, several rays are randomly generated onto the inclined heliostat surface. Nevertheless, in this case, a part of the heliostats can be already shadowed or blocked by other interfering heliostats. To not overestimate the SR shadow performance, the random rays considered are only the ones laying on the free mirror surface. So, the generated rays, with sun direction defined by $\hat{\mathbf{s}}_\mathbf{i}$ are then intersected with an infinite hyperboloid. The shadow performance was then evaluated as Equation 6.

$$\eta_{s,SR,i} = 1 - \frac{N_{in}}{N_{tot}} \quad (6)$$

Where N_{in} is the number of rays that fall inside the given hyperboloid shape while N_{tot} is the total number of rays generated on the heliostat surface.

2.1.2 SR section creation

Nowadays existent beam down solar application makes use of a circular field of heliostat and so circular secondary reflector. To unconstrain the shape of the hyperboloid, the field was divided into sections.

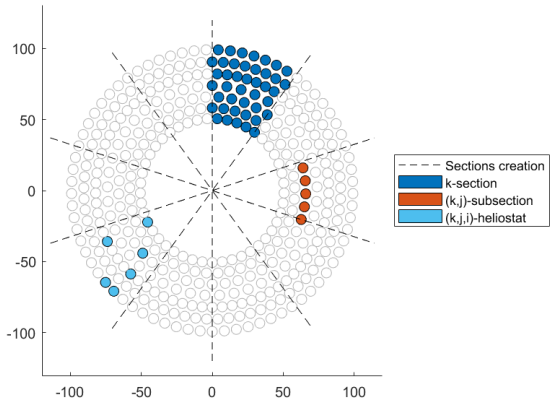

Figure 5: Section division methodology.

As shown in Figure 5, a section is defined as a circular sector of the field bounded by two angles. Every k-section is then formed by J-rows that are the maximum number of rows present in a field bounded by a minimum and maximum solar site radius. Every row of the field will be called a j-row, so every subsection can be defined by a combination (k, j). The number of sections must be even, bounded between the minimum value of 2 and the maximum one defined by the azimuth distance between two heliostats in the first row. The field was then divided into K-sections of equal azimuth range $360°/K$. A common j-row hyperboloid shape was considered, defined by a minimum and maximum radius, r_j and R_j and azimuth angle extension, ΔAz. These three characteristics were obtained by the intercept factor calculation presented before. For each i-heliostat it's possible to assess a circular sector of the hyperboloid based on the minimum and maximum radius, $r_{k,j,i}$ and $R_{k,j,i}$, and the azimuth angle extension $\Delta Az_{k,j,i}$, from a random bunch of ray generated at the inclined heliostat surface. For each (k, j)-subsection is then possible to evaluate $r_{k,j}$, $R_{k,j}$ and a $\Delta Az_{k,j}$ of the hyperboloid as the minimum and maximum values among all the I-heliostat present in the (k, j)-subsection. A common value of r_j and R_j was selected as the minimum and maximum radius found among all the K-section of a certain j-row of the field. The angle extension, on the other hand, was selected as the maximum one between all the $(K \cdot J)$-subsections. The final secondary reflector shape is then the union of all the K circular sectors.
In this work, a number of sections equal to 12 were considered in order to limit the superposition of a slice of hyperboloid to the axis of symmetry of the adjacent k-section.

2.1.3 Design field performance

In order to build a 50 MW_{th}, at receiver aperture, solar field at a given latitude, a Matlab model was built. The first task computed by the program is the radial staggered field layout between the minimum and maximum radius of the field selected. Then the sun position at the chosen design day is evaluated. The first best efficient (k, j)-subsection is considered and inserted into the field. The selection criteria is based on the mean DNI annual weighted cosine and intercept efficiency of every subsection. The choice acts on half of the field to obtain regularity on the final field layout and faster computational time. The subsection selection continues till the design power is reached. Subsequently, the secondary reflector shape is created and the shadow efficiency for the chosen mirrors is performed, so a new field instant power. If the latter is higher than the design one, the program performs the shadowing and blocking efficiency for each mirror, otherwise, the subsection selection continues. Again, the new power is compared to the selected one and the iterative process continues till the target is reached.

2.1.4 Receiver thermal losses

The ray path concludes at the receiver aperture where a Heat Transfer Fluid (HTF) is heated up and either stored or used as a hot source in a bottom power cycle. The CPC, if present, was considered a perfect reflector. Following the NREL Gen3 road map [33], a particle receiver was assumed. The radiative heat transfer will only consider the particles absorbed power, their emission, and reflection. It was assumed that the HTF act as a grey opaque body, with hemispherical emissivity equal to 0.9 [51]. The convective loss is mainly gravity-driven since the wind is limited to reduce material loss. Furthermore, this model assumes that if the CPC is built on an array configuration, each tertiary concentrator has its own receiver. Finally, the overall system efficiency, η_{sys}, can then be evaluated as Equation 7.

$$\eta_{sys} = \eta_{opt} \cdot \eta_{th} \tag{7}$$

Where η_{th} is the receiver thermal efficiency.

2.1.5 Clear sky model

A DNI clear sky model was utilized to evaluate the annual performances of a solar field. Considering every hour of the year, the annual field performance simulation can be computationally expensive. Instead, just a subset of hours can be assessed with sufficient accuracy [46]. For that reason, it was decided to simulate the field at every 15^{th} of each month of the year. The day hours were selected such that the sun elevation is higher than 15° [26].

2.1.6 SR shadow optimization

The SR shadow sensibly affects the annual optical field efficiency, as shown in Figure 6.

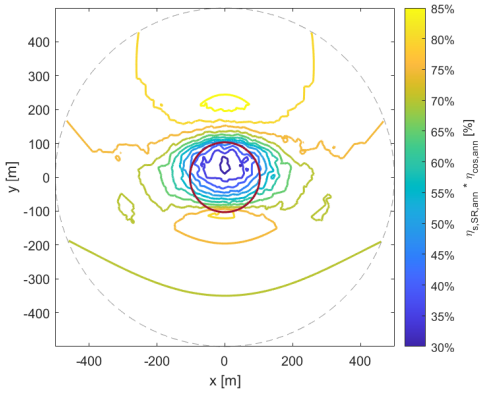

Figure 6: Annual clear sky DNI weighted efficiency (cosine and hyperboloid shadow) at ground level. Hyperboloid (red line) with eccentricity equal to 4. Aim point equal to 100 m. Latitude of 25° N.

The inner field part reaches annual cosine and secondary reflector shadow efficiency below 40%.
So, a Matlab optimization procedure was built aiming to maximize the overall optical efficiency at a given CPC geometry. Starting from the design solar field created, a new possible best efficient (k, j)-subsection is considered. The field is step by step thinned out, from the inner rows to the outward ones, of the worst annual efficient subsection till again the design power is reached. If the annual optical performance increases, a new optimized configuration is found. The iterative process continues till a maximum $\eta_{opt,ann}$ is attained.

2.1.7 Annual system optimization

The increased optical performances caused by the annual shadow optimization cannot neglect the thermal receiver ones. Higher $CR_{cpc,3D}$ and lower inlet radius, R_{cpc}, of the CPC can sensibly boost the thermal efficiency, but on the other hand limit the selection of farthermost, less shaded, heliostats due to low intercept factor. Moreover at low eccentricity values, the error amplification effects cause a bigger ground image, but, on the other hand, higher $CR_{cpc,3D}$. The opposite trend holds for high eccentricity values.
So an overall system optimization was proposed for an eccentricity values range from 1.5 to 4, aim point height equal to 100 m and 120 m, and receiver temperature of 750 °C [33].
The design DNI was considered equal to 1 kW/m^2.
First and foremost, a plausible CPC geometry needs to be found at every eccentricity and aim point height. These characteristics were established by analyzing the ground image of a simplified surrounded field configuration. An intercept value of 99% was considered, determining both R_{cpc} and maximum acceptance angle. Table 2 summarized the CPC geometry found for an aim point equal to 100 m.

e [-]	**1.5**	**2**	**2.5**	**3**	**3.5**	**4**
R_{cpc} [m]	18.2	11.2	9.2	8.4	8.0	8.1
$CR_{cpc,3D}$ [-]	6.92	4.15	2.90	2.35	1.80	1.75

Table 2: Surrounded field configuration CPC geometry. Aim point equal to 100 m.

Then, at a given eccentricity and aim point height, the base CPC geometry is varied, reducing and increasing the starting values of both $CR_{cpc,3D}$ and R_{cpc} by a selected interval dimension. Every new configuration is assessed, and the iterative process continues till the first CPC geometry that maximizes the annual system efficiency is found.

2.1.8 Techno-economic ananlysis

A techno-economic model was built in order to justify system performance results also in terms of Levelized Cost Of Heat (LCOH). The LCOH evaluated considers constant annual energy production and Operation and Maintenance (O&M) cost over the lifetime chosen (25 years) [2]. The procedure is based on a before-tax-revenues approach, so no tax and no financing were considered. With these assumptions, the LCOH can be evaluated as Equation 8 [44].

$$LCOH = \frac{I \cdot FCR}{E} + \frac{O\&M}{E} \tag{8}$$

Where I is the overnight investment, FCR is the Fixed Charge Rate, E is the annual thermal energy output. In order to compare the results with the literature, the same clear sky system annual performance was considered, but the energy produced will be given by an averaged annual DNI of 7 kWh/day/m^2 and 365 days of annual operation. The tower cost was considered equal to the one found for a solar tower, but in this case, the installation height was taken equal to the one attained by the hyperboloid vertex point. Furthermore, the same specific cost of the heliostats was considered for the secondary reflector mirror facets. Since no articles were found regarding the cost of the CPC, the receiver cost has been increased by 10%.

Lifetime	25 years [2]
DNI	7 kWh/day/m^2 [35]
Discount rate	9 % [2]
O&M	0.023 €/kWh$_{th}$ [2]
EPC & Cont.	40% of the investment [4]
Field cost	9100 €/acre
Tower cost	$2.73 \cdot 10^6\ e^{0.0113\ TH}$ €
Receiver cost	113 (1+10%) €/kW$_{th}$ [33]
Heliostat cost	132 €/m^2

Table 3: Beam down optic LCOH evaluation assumptions. Field, tower and heliostat cost from SolarPILOT default values.

2.2. SR thermal model

A 1D thermal model of the hyperboloid was built to assess the temperature distribution on the SR. As figured in Figure 9, the heat flux can reach levels up to 18 kW/m^2.

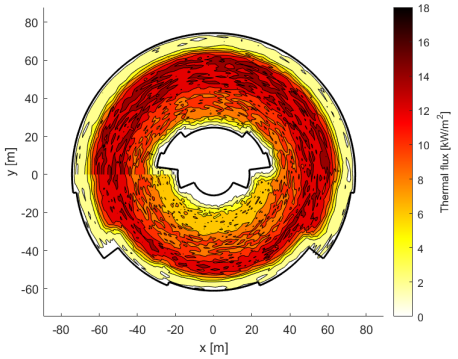

Figure 7: SR heliostats radiation heat flux at aim point equal to 120 m and eccentricity of 3.

Highly reflective surfaces are generally made by a thin silver film covered with glass in order to avoid the fouling degradation effect. An example of the solar film is the one proposed by 3M^{TM}, called Solar Mirror Film 1100. The type of glass utilized by the Weizmann Institute of science is the SCHOOT Borofloat 33 [5]. It can be modeled as a semi-transparent grey body across most of the spectrum, while an opaque grey body in the other. The downwards facing part of the hyperboloid is then completed as the union glass-silver facets. Moreover, the maximum operating temperature is imposed by the silver surfaces, 65 °C, since the glass one is 450 °C [17][41].
The upward-facing surface, on the other hand, has to dissipate the high thermal flux coming from the heliostats field and the direct sun radiation. Two different configurations were individuated by the Weizmann Institute, a sandwich configuration, in which two silver-glass modules are stick one to each other, or an aluminium finned one, in order to increase the heat transfer area on the upper part of the hyperboloid. Furthermore, two other configurations were added to this work. If fins are not installed, only the aluminium fin support was considered and the solution can be comparable to the one of the sandwich type. Moreover, the latter configuration can be further improved with the installation of dry cooling technology. A heat contribution is withdrawn from the upward-facing surface to limit the operating value of the silver temperature.
The nature of the heat transfer is of a convective, conductive, and radiative type. For simplicity, the hyperboloid was treated as a horizontal flat surface with a unitary view factor on both sides, respectively with the ground and the sky.

Radiative heat transfer Following the Fresnel refraction law and the Snell law, the reflectivity of a glass surface facing air for normal incoming radiation can be evaluated as Equation 9 [18].

$$\rho_g = \left(\frac{n_g - 1}{n_g + 1}\right)^2 \tag{9}$$

Where n_g is the refractive index of the glass and it's considered constant among the spectrum. The effective radiative properties of the glass can be predicted by an analytical ray-trace approach. So, the absorbance property of the glass in the glass transparent band, α_g^T, can then be evaluated thanks to Equation 10.

$$\alpha_g^T = \frac{(1-\tau_g)(1-\rho_g)(1+\rho_s\tau_g)}{1 - r_g\rho_s\tau_g^2} \tag{10}$$

Where τ is the transmittance and ρ is the reflectivity and the subscript g refers to the glass, while s to the silver surface. Furthermore, it was assumed that half of the contribution acts on the outer glass surface while the other half is on the silver surface.

The silver absorbance property in the glass transparent band can then be performed as the non-reflected part of the radiation at the lower glass side.

$$\alpha_s^T = \frac{\tau_g(1-\rho_s)(1-r_g)}{1 - r_g\rho_s\tau_g^2} \tag{11}$$

In the glass transparent band, the net contribution on the glass surface is equal to the absorbed incidence radiation and the emission in that spectrum. However, the latter factor is negligible since the emissivity is close to zero in the considered wavelength range. On the other hand, the silver surface it's opaque and so its net contribution it's pure of absorption and emission type. The latter can again be neglected due to its high reflectivity value.
Furthermore, in the opaque glass spectrum, the net contribution on the outer glass surface is given by the difference between the absorption of the incident radiation and emission as a grey body. The net radiative contribution on the silver surface is zero.

Convective heat transfer The convective heat transfer phenomena can be of a free or forced type. The strength of natural convection is mainly governed by buoyancy expressed by the Grashof number Gr_L while the forced convection is characterized by the Reynolds number Re_L, with L a characteristic length. When $Gr_L/Re_L^2 \ll 1$, the forced convection dominates and the opposite for $Gr_L/Re_L^2 \gg 1$. If the two dimensionless numbers are comparable we have a mixed convection process. In this case, the heat transfer coefficient can be roughly estimated as the maximum one between both [38]. The free convection is strictly dependent on the plate orientation and inclination. In the finned configuration, two different surfaces participate in the convective dissipation, namely the aluminium horizontal support and the fin extension. The convective heat loss from a fin can be evaluated considering the differential equation solution for a non-isothermal fin with an adiabatic tip. The fin height, H, was considered equal to 50 cm in order to limit the product mH at 3 at stagnant air condition. Where $m = \sqrt{2h/kt_f}$, with h the natural convective heat transfer coefficient, k the aluminium conductivity and t_f the fin thickness.

Energy balance Four nodes were identified in every configuration. In the sandwich one, the two outer glass surfaces and the two silver ones. In the finned or not finned configuration, are the outer downward facing glass surface, the silver surface, the inner and outer upward-facing metal surface. The temperature solution can then be performed by solving the heat transfer balance at each of the four nodes.
For the cooled configuration, the silver temperature was set to its maximum limit, and the refrigeration power was estimated.

3. Results

3.1. Heliostat field creation

The best heliostats field configuration was found at eccentricity equal to 2, in both aim point simulations. For tower height equal to 100 m, the annual system efficiency of the optimized configuration settles down to 59.32%, the product of annual optical efficiency of 68.45%, and annual thermal efficiency of 86.67%. The system performance increases by 1.90% relative to the base configuration. The R_{cpc} settles down to a value of 11.2 m while the $CR_{cpc,3D}$ is 3.65.
At the aim point equal to 120 m, the increased cosine and thermal performances (caused by a higher CPC concentration ratio) boost the overall solar field system efficiency to a value of 61.07%.
Starting from the base configuration the CPC inlet radius reduces in every simulation, as a trade-off between thermal and intercept performances. The $CR_{cpc,3D}$ follows the same trend as a balance between optimized hyperboloid shadow, cosine, and intercept efficiency.
At low eccentricity (e<2.5), the optimized CPC geometry differs a lot from the base configuration. Error amplification effect causes too big ground image and although the $CR_{cpc,3D}$ obtained was higher with respect to bigger eccentricity values, the optimization sensibly reduces the intercept factor aiming at better thermal performances.

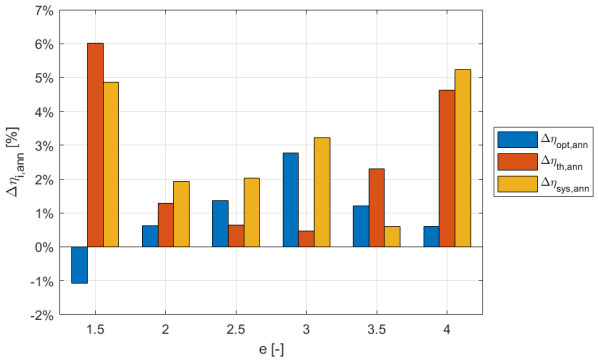

Figure 8: Relative percentage optical, thermal, and system annual efficiencies increase from base to optimized configuration. Aim point equal to 120 m.

The same consideration can be made at a high eccentricity value (e>3), where the $CR_{cpc,3D}$ is strongly limiting the thermal receiver performance. The hyperboloid shadow efficiency, at an aim point equal to 100 m, reaches a value of 90% in the base configuration and eccentricity equal to 4. The field is optimized by selecting farther heliostats so to settle down this value around 95%. The CPC inlet radius is reduced as a trade-off of decreased intercept and boosted thermal performances. Nevertheless, the field optical performance is almost constant while the thermal efficiency increase over 4% relative to the base case. The overall annual efficiency attains the highest variation, compared to other eccentricity values, with a 5% relative increase with respect to the base case.
At eccentricity equal to 3, the optimization is almost field-driven. The CPC geometry slightly changes and so do the thermal performances. On the other hand, the field optical efficiency is boosted, passing from 65.30% to 67.11% at an aim point equal to 100 m, mainly driven by a 3.5% relative SR shadow efficiency increase.

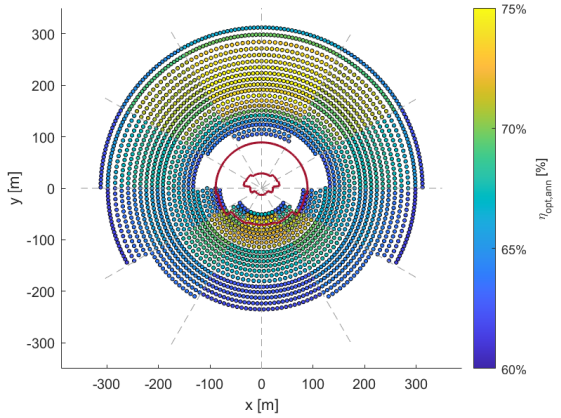

Figure 9: Optimized heliostats field configuration at eccentricity equal to 3 and aim point equal to 120 m.

In every configuration, the annual field optimization reduces the hyperboloid area. The highest variation is obtained at eccentricity equal to 3 and aim point equal to 120 m, with a reduction of around 1000 m^2. The overall field concentration ratio, at eccentricity equal to 2, reaches a value of 749.6 at aim point equal to 100 m and 827.8 at 120 m.
The best techno-economic configuration is found for eccentricity equal to 3 and an aim point of 120 m with an LCOH of 57 €/MWh_{th}. The eccentricity value of 2 and the same aim point height, namely the best field configuration found in terms of annual system performance, is affected by higher tower costs. The tower height at the best techno-economic configuration decreases from 94 m to 85 m. At an aim point equal to 150 m, the tower cost increase does not justify the better field performances and the LCOH is the highest at every eccentricities.
The annual thermal energy produced by the best techno-economic configuration is 100.85 TWh_{th}. These results are comparable to what was presented by Ali Hussaini et al. for a 50 MW_{th} conventional solar tower in Nigeria (latitude of 12.4°). They found an LCOH around 36 €/MWh_{th}, but the design DNI was taken equal to 670 kW/m^2 and so a higher reflective area is attained with an annual thermal generation of 150.77 TWh_{th}, assuming an annual averaged DNI of 5.5 kWh/day/m^2 and aim point equal to 100 m [2]. Moreover, also the mean DNI annual system

efficiencies are comparable, 59.49% obtained by the beam down optimization and 54.80% for the solar tower. Nevertheless, the lower design DNI value considered for the conventional solar tower application can sensibly reduce the annual performances.

3.2. SR thermal model

For heliostats radiation heat flux over 7 kW/m^2 and stagnant air, no configuration is valuable to limit the silver temperature under its maximum operating value. As shown in Figure 10, a cooling technology needs to be adopted.

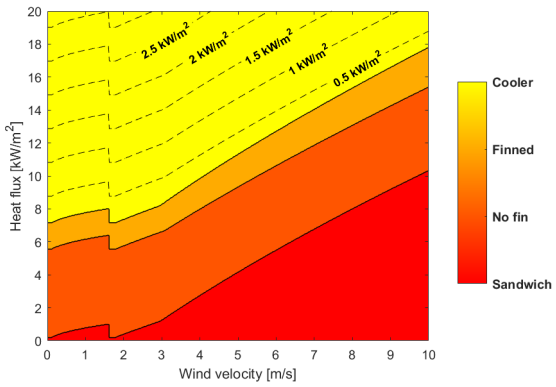

Figure 10: Secondary reflector possible configuration to limit the silver temperature at 65 °C. Dashed isoline represent the refrigeration power.

The metal configuration performs better than the sandwich one in both cases, namely with and without fins. Due to the high reflectivity and conductivity of aluminum, the upward-facing surface dissipation is favored both in terms of radiative and convective heat transfer.
The results are influenced by the characteristic length considered, namely 1 m. Nevertheless, considering a characteristic length of 50 m, the relative error on the results is lower than 10% on the silver temperature. So, the analysis can be considered a good first value in analyzing the secondary reflector behavior per meter square of surface.
At the aim point equal to 120 m, the overall refrigeration heat is 4.54 MW and 5.38 MW, respectively at eccentricity equal to 2 and 3. By increasing the silver limiting operation temperature to 150 °C, the latter values settle down at 2.63 MW and 2.74 MW.

$\dot{\mathbf{Q}}_{\mathbf{refr}}$ [MW]	$T_{silver,lim}$		
	65 °C	**100 °C**	**150 °C**
e = 2	4.54	4.18	2.63
e = 3	5.38	4.99	2.74

Table 4: Refrigerant power in order to keep the silver temperature under its limiting condition.

4. Conclusions

A 50 MW$_{th}$ BD optimized solar field was presented. The results were presented for 25° N of latitude, but the algorithm can be applied to any solar site.
Starting from a simplified surrounded field configuration, a first CPC geometry was found and the optical and thermal performances were assessed at different eccentricity and aim point values. An annual optimization model was built as a compromise between the CPC geometry and the SR shadow performance. The receiver temperature was assumed to equal 750 °C. The best BD configuration in terms of LCOH was found at eccentricity equal to 3 and an aim point of 120 m. In this case, the optimization is mainly optical driven, caused by a 3.5% relative percentage increase in the annual shadow hyperboloid efficiency concerning the surrounded field configuration. The field shape becomes slightly asymmetric, and north-oriented, resulting in an annual optical efficiency of 65.08% and a thermal of 87.96%. The CPC inlet radius settles down to a value of 7.9 m and the $CR_{cpc,3D}$ is 2.50. The number of the mirror reduces from 2755 to 2654 and the same trend is followed by the SR area which decreases by 12% relative. The annual energy produced is 100.85 TWh$_{th}$ at averaged annual DNI of 7 kWh/day/m^2. The LCOH settles down at value of 57 €/MWh$_{th}$.
Furthermore, a 1D SR thermal model was presented. Different SR configurations were studied, namely the sandwich, the finned or not one, and the possibility of dry cooling technology. At the best techno-economic configuration, if the silver temperature is limited to 65 °C, 45% of the hyperboloid surface needs to be cooled down. If the silver temperature limit can be increased up to 150 °C, this value reduces to 14%. In the latter case, the fin configuration occupies another 14%, the not finned one the 22.5 %, and in the remaining part a sandwich configuration can be utilized.
The model presented lacks of accurate analysis in the receiver thermal behaviour and CPC optic. In this sense, a suitable configuration of particle receivers needs still to be directly associated and the thermal model deeply assessed. Moreover, an accurate approach for the CPC transmissivity efficiency can be accompanied in order to improve the accuracy of the intercept efficiency calculation. Scaling up beam down solar system needs to take into account the thermo-mechanical stress on the hyperboloid surface. So, a 3D thermal model needs to be considered in order to properly analyze the heat flux distribution. The design power will then be a compromise between the refrigeration heat, material utilized and energy produced.
The number of each reference used in the text refers to the bibliography of the thesis.